Hydrogen Adsorption on Functionalized Nanoporous Activated Carbons

X. B. Zhao, B. Xiao, A. J. Fletcher, and K. M. Thomas*

Northern Carbon Research Laboratories, School of Natural Sciences, Bedson Building, University of Newcastle upon Tyne, Newcastle upon Tyne, NE1 7RU, U.K.

Received: January 6, 2005; In Final Form: March 1, 2005

There is considerable interest in hydrogen adsorption on carbon nanotubes and porous carbons as a method of storage for transport and related energy applications. This investigation has involved a systematic investigation of the role of functional groups and porous structure characteristics in determining the hydrogen adsorption characteristics of porous carbons. Suites of carbons were prepared with a wide range of nitrogen and oxygen contents and types of functional groups to investigate their effect on hydrogen adsorption. The porous structures of the carbons were characterized by nitrogen (77 K) and carbon dioxide (273 K) adsorption methods. Hydrogen adsorption isotherms were studied at 77 K and pressure up to 100 kPa. All the isotherms were Type I in the IUPAC classification scheme. Hydrogen isobars indicated that the adsorption of hydrogen is very temperature dependent with little or no hydrogen adsorption above 195 K. The isosteric enthalpies of adsorption at zero surface coverage were obtained using a virial equation, while the values at various surface coverages were obtained from the van't Hoff isochore. The values were in the range 3.9−5.2 kJ mol^{-1} for the carbons studied. The thermodynamics of the adsorption process are discussed in relation to temperature limitations for hydrogen storage applications. The maximum amounts of hydrogen adsorbed correlated with the micropore volume obtained from extrapolation of the Dubinin−Radushkevich equation for carbon dioxide adsorption. Functional groups have a small detrimental effect on hydrogen adsorption, and this is related to decreased adsorbate−adsorbent and increased adsorbate−adsorbate interactions.

1. Introduction

Hydrogen is a possible replacement for fossil fuels as a low-emission energy carrier.[1] However, the widespread use of hydrogen as a fuel is limited by the lack of a convenient and cost-effective method of hydrogen storage, which is a crucial step for providing a supply of hydrogen fuel for end use. The following hydrogen storage options are available: a) metal hydrides, b) adsorption on porous materials, and c) compressed gas. None of these approaches currently satisfy all the criteria of the storage capacity, size, efficiency, cost, and safety required for use in transportation applications. It is envisaged that an adsorbent material consisting exclusively of pores with molecular dimensions (<0.5 nm) could adsorb sufficient hydrogen, at significantly lower pressures than those used for compressed gas, to meet the requirements for transportation use. Current DOE hydrogen storage targets are 4.5 wt% by 2005, 6 wt% by 2010, and 9 wt% by 2015.[1]

Initial studies[2−5] of hydrogen adsorption on graphitic fibers, carbon nanotubes, and porous carbons showed high uptakes, but recent work has cast doubt on earlier observations.[6−11] Current carbon adsorbents afford only small amounts of hydrogen adsorption even at 10 MPa.[9] Porous carbons are amorphous materials which contain both hydrophobic graphene layers and hydrophilic functional groups.[12,13] The pore size distribution in these materials may be tuned from a structure with porosity almost exclusively <2 nm, to include meso- and macroporosity. The maximum amounts of hydrogen adsorbed on porous carbons correlate with surface area determined by gas adsorption methods, whereas hydrogen adsorption on porous metal organic framework materials has more complex characteristics.[12−15] In the case of hydrogen adsorption on nanoporous metal organic framework materials formed by using methanol and ethanol templates with $Ni_2(bipy)_3(NO_3)_4$, the hydrogen may be 'kinetically trapped' in the porous structure at 77 K and is released gradually above 110 K.[16] This kinetic trapping effect is related to the flexibility of the porous framework materials.[16]

Adsorption of supercritical hydrogen is limited by the low interaction energy between hydrogen and carbon surfaces, which is only enhanced in porosity where the pore dimensions are similar to those of hydrogen. Enhancement of the fundamentally weak physisorption interaction between carbon surfaces and the poorly polarizable H_2 molecule, at temperatures well above its critical temperature (T_c = 33 K), is challenging and requires new approaches to optimize the physisorption interaction to compete with thermal energies. There is an intrinsic conflict between the large pore volume required to enhance hydrogen storage capacity and the resulting decrease in the adsorbate/adsorbent interaction energy in wider pores.

A possible way of developing new hydrogen storage materials has been identified as functionalized nanocarbon materials with improved storage properties compared with nonfunctionalized counterparts.[1] Functional groups may have either electron-withdrawing or -donating effects on the graphene layers in activated carbons, which may influence hydrogen adsorption. In this study, the incorporation and modification of oxygen and nitrogen functional groups were carried out in two main series of carbons so that the porous structure did not vary significantly within a given series, thereby allowing the influence of functional groups on hydrogen adsorption to be separated from those of porous structure. The effects of functional groups,

* Author to whom correspondence should be addressed. Email: mark.thomas@ncl.ac.uk.

10.1021/jp050080z CCC: $30.25
Published on Web 04/14/2005

porous structure characteristics, and temperature on hydrogen adsorption on functionalized nanoporous activated carbons were investigated to study the optimization of carbon surfaces characteristics for hydrogen adsorption.

2. Experimental Section

2.1. Carbon Precursor Materials Used. *2.1.1. Activated Carbon Materials Used.* Commercially available coconut shell-derived carbons G209, G210, and G212, prepared by physical activation using steam at 1173 K, were used in this study. These carbons were supplied by Pica, Vierzon, France.

2.1.2. Polyacrylonitrile (PAN)-Derived Carbon. Polyacrylonitrile (PAN) powder supplied by Aldrich Chemicals was pretreated in air at 473 K for 1 h. The pretreated PAN was heated at a rate of 3 K min^{-1} to 1173 K in argon. The argon flow was then changed to carbon dioxide, and the char was gasified at 1173 K for 4 h. This gave a carbon, designated code PANC, which had a burnoff of ~60 wt%.

2.1.3. Sodium Carbonate Activation Procedure. A mixture of 75 g of sodium carbonate and 25 g of PAN was prepared. This was preoxidized at 473 K for 1 h under air with flow rate of 10 cm^3 min^{-1}. The sample was heated to 1173 K at a heating rate of 10 K min^{-1} in helium gas (flow rate 20 cm^3 min^{-1}). The carbon sample was cooled to room temperature under helium gas. The carbon was finally crushed and sieved. The 0.7−1.7 mm fraction was extracted using a Soxhlet apparatus for 72 h, using 400 mL of water to remove soluble material. The carbon was then dried at 388 K in air for 72 h. This carbon sample was designated PAN−Na carbon.

2.2. Treatment Procedures. *2.2.1. Chemical Oxidation Treatment.* The PANC and G209 carbons were chemically modified by oxidation using nitric acid in order to introduce various oxygen functional groups on the carbon surface. Carbons G209 and PANC were refluxed in 7.5 M HNO_3 solution for 48 h. The oxidized carbons were Soxhlet-extracted with water, until the pH of the aqueous extract was constant, to remove residual HNO_3 and any soluble materials. The carbons were dried under vacuum at 348 K. The resultant carbons derived from PANC and G209 were designated sample codes PANCN and GN, respectively.

2.2.2. Heat Treatment Procedures. Carbons PANCN and GN were heat-treated to provide a suite of carbons where the oxygen functional groups with various thermal stabilities were varied progressively. The carbon samples were heated at 3 K min^{-1} and held at the heat treatment temperature (HTT) for 1 h. The resultant carbons were designated using the code of original carbon followed by a number to indicate the HTT in K, e.g. GN573 represents GN heat treated to 573 K and held at the HTT for 1 h. Similarly PANCN673 represents PANCN heat treated to 673 K and held at this temperature for 1 h.

2.3. Analytical Measurements. Carbon, hydrogen, nitrogen, and oxygen analyses were determined by Microanalytical Services, Oakhampton, UK.

2.4. Adsorption Studies. *2.4.1. Gases.* Hydrogen (ultrapure plus grade, 99.9999%) was supplied by Air Products, UK. Nitrogen (99.9995%), carbon dioxide (99.999%), and deuterium (99.98% D_2) were supplied by BOC, UK.

2.4.2. Isotherms and Kinetics. An intelligent gravimetric analyzer (IGA) supplied by Hiden Analytical Ltd, UK, was used in this study. This apparatus is an ultrahigh vacuum system (UHV), which allows isotherms and the corresponding kinetics of adsorption and desorption to be determined, for set pressure steps.[17−18] Hydrogen and deuterium were purified using an adsorbent trap at 195 K. The samples (100 ± 1 mg) were outgassed at 473 K and ~1×10^{-5} Pa bar until no further weight loss was observed. The temperature of the balance and pressure control system was controlled ±0.2 K to eliminate changes in the external environment. The microbalance had a long-term stability of ±1 μg with a weighing resolution of 0.2 μg. The sample temperature for hydrogen and nitrogen adsorption was achieved using an extended quartz sample vessel and hangdown with liquid nitrogen in a Dewar flask. The sample temperature was monitored using a platinum resistance thermocouple throughout the experiment, and the variation in sample temperature was minimal (<0.1 K). The initial cooling of the quartz vessel in liquid nitrogen under UHV gave a temperature of ~140 K. The first pressure increment involves a change from UHV to gas at low pressure, and this introduces conduction through the gas phase at 1 mbar to the sample, which results in cooling to 77 K. The gas pressure was gradually increased, over a timescale of ~30 s to prevent disruption of the microbalance, until the desired value was achieved. Pressure control was via the use of three transducers with ranges 0−0.2, 0−10, and 0−100 kPa, each with an accuracy of 0.02% of the specified range. The pressure was maintained at the set point by active computer control of the inlet/outlet valves throughout the duration of the experiment. The mass uptake was measured as a function of time, and the approach to equilibrium of the mass relaxation curve monitored in real time using a computer algorithm. In the case of hydrogen/deuterium adsorption or desorption, equilibrium was established very quickly (<2 min). However, each point was allowed a minimum equilibration time of 15 min. The hydrogen adsorption kinetics were too fast, relative to the time for the pressure step to take place, to allow accurate measurement of the adsorption kinetics. A platinum resistance thermocouple located very close (<5 mm) to the sample showed no temperature changes resulting from the pressure increments. Buoyancy corrections were carried out using the weights and densities of all the components of the sample and counterweight sides of the balance and the measured temperature. The hydrogen density at the triple point (0.077 g cm^{-3}) was used for the density of adsorbed hydrogen. Isobars were measured by first adsorbing hydrogen at 77 K at a set pressure. The sample was then allowed to warm by natural evaporation of the liquid nitrogen. The temperature−time profile was monitored throughout the process. This showed that the heating rate was typically ~0.3 K min^{-1}. The adsorption kinetics are fast, and therefore, equilibrium is achieved on this time scale.

The saturated vapor pressures were calculated using the following equation[19]

$$\log_{10} p = A - \frac{B}{T + C} \quad (1)$$

where p is the saturated vapor pressure (Torr), T is the temperature in °C, and A, B and C are constants defined by the adsorbate: nitrogen (77−373 K) $A = 6.49457$, $B = 255.68$, $C = 266.550$, carbon dioxide (77−303 K): $A = 7.810237$, $B = 995.7048$, $C = 293.4754$.

3. Results and Discussion

3.1. Analytical Data. The analytical data for the nanoporous activated carbons used in this study are given in Table 1. The oxygen contents of the low-nitrogen-content G suite of carbons varied from ~3 to 22 wt% daf, while the high (7−8 wt% daf)-nitrogen-content PAN series varied in the range ~2−20 wt% daf oxygen. It is apparent that both series have low ash contents and are very similar except for the consistent high nitrogen content in the PAN series of carbons. The other activated carbons have typical analytical data for porous carbon materials.

TABLE 1: Analytical Data for the Carbons Used in This Study

	proximate analyses		elemental analyses, wt% daf				atomic ratio ×100		
carbon samples	V[a]	A[b]	C	H	N	O	N/C	H/C	O/C
				G series					
GN	33.77	0.49	76.34	0.89	1.05	22.36	1.18	13.99	21.97
GN573	29.66	0.23	79.45	0.74	1.07	17.21	1.15	11.18	16.25
GN673	19.68	0.92	83.94	0.63	1.05	13.65	1.07	9.01	12.20
GN773	17.92	0.76	85.64	0.71	1.10	12.87	1.10	9.95	11.27
GN873	13.18	0.66	89.28	0.52	1.17	9.00	1.12	6.99	7.56
GN1073	5.20	0.84	94.03	0.49	1.24	3.56	1.13	6.25	2.84
G209	4.46	2.73	96.22	0.42	0.28	2.95	0.25	5.24	2.29
G210	3.32	1.78	97.57	0.27	0	2.13	0	3.31	1.64
G212	3.15	3.25	99.14	0.24	0	1.95	0	2.91	1.48
				PAN series					
PANCN	26.64	0.45	72.66	0.99	7.55	19.75	8.91	16.37	20.37
PANCN573	18.72	0.35	75.55	0.85	7.94	14.22	9.01	13.50	14.12
PANCN673	16.28	0.42	77.07	0.95	8.16	13.40	9.08	14.79	13.04
PANCN873	10.27	0.32	82.33	0.93	8.70	7.99	9.06	13.56	7.28
PANCN1073	9.11	0.18	83.28	1.10	7.77	6.40	8.00	15.86	5.76
PANC	1.03	0.70	89.28	0.37	8.19	2.18	7.86	4.97	1.83
PAN−Na	4.91	0.63	88.28	1.08	1.76	6.42	1.71	14.69	5.46

[a] Volatile content, %daf; daf = dry ash free. [b] Ash content, %db, db = dry basis.

TABLE 2: Porous Structure Characterization Data for the Carbons Used in This Study[a]

PAN series carbons	V_{CO_2}[b], cm^3 g^{-1}	V_{N_2}[c], cm^3 g^{-1}	G series carbons	V_{CO_2}[b], cm^3 g^{-1}	V_{N_2}[c], cm^3 g^{-1}
PANCN	0.112	0.181	GN	0.262	0.366
PANCN573	0.141	0.213	GN573	0.258	0.413
PANCN673	0.127	0.216	GN673	0.235	0.443
PANCN873	0.148	0.236	GN773	0.234	0.448
PANCN1073	0.121	0.231	GN873	0.225	0.455
PANC	0.153	0.204	GN1073	0.260	0.503
PAN−Na	0.311	0.466	G209	0.334	0.484
			G210	0.331	0.442
			G212	0.346	0.741

[a] Density of adsorbed phase (g cm^{-3}): nitrogen, 0.8081; carbon dioxide, 1.023. [b] Obtained from intercept of DR plot. [c] Obtained from Langmuir model at $p/p^0 = 1$.

3.2. Functional Group Characterization. It is only possible to incorporate mixtures of functional groups into porous carbons, and it is difficult to quantify functional-group surface compositions because of the range of structural environments in these amorphous materials.[20] In this study, the functional groups were incorporated by nitric acid oxidation. The oxygen functional groups have varying thermal stabilities and decompose progressively during heat treatment with desorption of CO and CO_2. The nitrogen functional groups behave differently during temperature programmed desorption (TPD) and are mainly converted to other functional groups in the structure rather than desorbed. The only exception is the pyridine *N*-oxide groups. The TPD results show that the decomposition ranges of the oxygen and nitrogen functional groups only overlap to a very limited extent. TPD studies provided quantitative overall CO_2/CO ratios for the carbons but estimation of functional groups by this method is only semiquantitative due to the need to use various assumptions to obtain functional group concentrations. The CO_2/CO ratios varied from 0.60 for GN and 0.79 for PANCN to 0.19 for GN673 and 0.11 for PANCN873.[21] The results are consistent with the following order of thermal stability: phenolic/semiquinone/carbonyl > lactone/lactol > −COOH for both the G and PAN series of carbons.

The acid/base titration results obtained using the Boehm method[22] for the G and PAN series of carbons have shown that all the functional groups decrease progressively with increasing heat treatment temperature.[21,22] The presence of basic nitrogen groups in the PAN carbons partly neutralizes the acidic groups decreasing the total acidity by ∼40%. Therefore, the titration data for the G and PAN series were not directly comparable.

The XANES spectrum of PANCN has peaks due to pyridinic, pyridone (or cyanide), and pyrrolic functional groups similar to PANC and an additional peak at ∼405 eV due to pyridine *N*-oxide surface species.[21] Heat treatment of PANCN to ≥673 K results in the complete disappearance of the pyridine *N*-oxide peak.[21] Relative concentrations of the pyridinic, pyridone (or cyanide), and pyrrolic functional groups and the nitrogen contents do not change significantly with heat treatment in the PAN series. The results were consistent with only relative minimal changes in surface nitrogen functional groups and concentrations, whereas the oxygen groups change to a greater extent (overall × 10) during heat treatment.

3.3. Porous Structure Characterization. The porous structures of the carbon materials were characterized using both nitrogen adsorption at 77 K and carbon dioxide adsorption at 273 K, and the results are given in Table 2. All the isotherms were Type I in the IUPAC classification scheme.[23] The micropore volumes of the microporous carbons were obtained using the Dubinin−Radushkevich (DR) equation,[24] which is as follows

$$\log n = \log n_0 - D \log^2(p^0/p) \qquad (2)$$

where n is the amount adsorbed at pressure p, n_0 is the amount adsorbed corresponding to the micropore volume, p^0 is the saturated vapor pressure, and D is a constant related to the microporous structure of the adsorbent.[24] An estimate of the micropore volume was obtained from extrapolation of the DR graph for CO_2 adsorption at 273 K to $p/p^0 = 1$. The total pore volume was obtained from the amount of nitrogen adsorbed at

77 K at $p/p^0 = 1$. The data in Table 2 show that the total and micropore volumes do not change greatly with heat treatment within both the G and PAN series of activated carbons. The total and micropore volumes of the PAN carbons (excluding PAN−Na) have averages of 0.214 ± 0.020 and 0.134 ± 0.016 $cm^3\ g^{-1}$, respectively, while the corresponding values for the GN−GN1073 series were 0.438 ± 0.046 and 0.246 ± 0.016 $cm^3\ g^{-1}$, respectively. The mean radii of microporosity, from the Dubinin−Stoeckli method,[25] of CO_2 adsorption data at 273 K were very similar within a given series with average values of 0.477 ± 0.022 and 0.306 ± 0.010 nm for the G and PAN series, respectively. Therefore, the effect of surface functional groups on the adsorption characteristics of a given series can be studied while excluding marked effects due to changes in porous structure within a given series. The other carbons are included to give a range of porous structure characteristics. Carbonization of PAN with sodium carbonate to give PAN−Na had a marked effect on the porous structure increasing both the micro- and total pore volumes by about two times and the mean radius of microporosity in PAN−Na to 0.40 nm while decreasing the nitrogen content to ~20% of the other PAN carbons.

3.4. Hydrogen Adsorption Isotherms. Hydrogen has a weak quadrupole, which may interact with surface groups. Functional groups may also influence the surface properties of the graphene layers. Therefore, changes in hydrogen adsorption characteristics may be expected with changes in surface functional group type and concentration.

The isotherms for adsorption and desorption of both hydrogen and deuterium by activated carbon G212 at 77 K are shown in Figure 1a. Both isotherms are Type I in the IUPAC classification scheme.[23] Consistency of these data with isobars and thermodynamic considerations described later represents the validation procedure for the experimental protocols. Both isotherms are reversible with virtually no hysteresis. The D_2 isotherm is slightly greater than the H_2 isotherm on a mole basis. This is attributed to competing quantum effects 1) the quantum-statistical mass effect on the vibrational energy levels normal to the surface and 2) the quantum-mechanical effect of isotopic substitution on the dispersion energy.[26] This difference suggests that quantum molecular sieving is possible in nanoporous materials. These observations confirm the accuracy of the adsorption isotherms.

All the hydrogen adsorption and desorption isotherms for functionalized PAN and G series carbons at 77 K were Type I with little or no hysteresis. These carbons have widely different porous structure and functional-group characteristics. Hydrogen adsorption isotherms for PANC, PANCN873, and PAN−Na at 77 K are given in the Supporting Information. These isotherms show hydrogen adsorption on a wide range of functionalized carbons.

Figure 1b shows the effect of temperature on hydrogen adsorption. It is apparent that temperature has a very marked effect on the hydrogen adsorption characteristics.

The Langmuir isotherm[27] can be expressed in the following form:

$$p/n = 1/n_m b + p/n_m \qquad (3)$$

where p is the pressure, n is the amount adsorbed, n_m is the monolayer capacity, and b is the coefficient of adsorption specific to the adsorbate/adsorbent system. Typical Langmuir graphs for hydrogen adsorption on carbons G212 and PANC at 77 K are shown in the Supporting Information (Figures SI 4 and SI 5). The graphs are linear in the region 15−100 kPa, thereby allowing accurate assessments of the maximum amounts

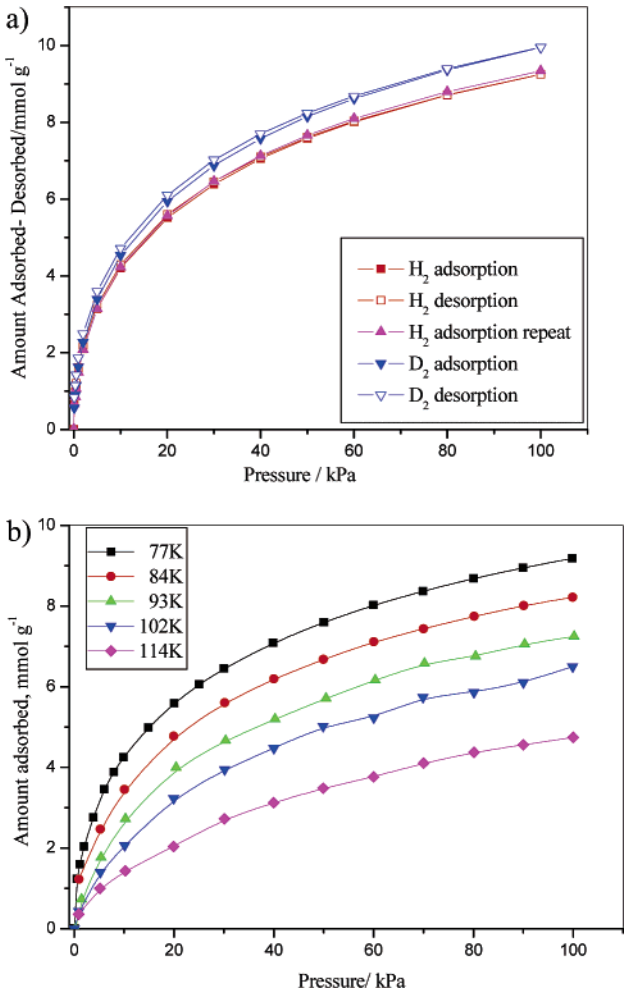

Figure 1. Isotherms for hydrogen and deuterium adsorption on activated carbon G212 (a) hydrogen and deuterium adsorption/desorption isotherms at 77 K (b) hydrogen adsorption isotherms: temperature range 77−114 K.

TABLE 3: Langmuir Parameters for Hydrogen Adsorption at 77 K on the Carbons Used in This Study

PAN series carbons	$H_2(n_m)$, mmol g^{-1}	G series carbons	$H_2(n_m)$, mmol g^{-1}
PANCN	2.89 ± 0.28	GN	5.85 ± 0.11
PANCN573	2.92 ± 0.31	GN573	6.21 ± 0.13
PANCN673	3.07 ± 0.25	GN673	6.55 ± 0.13
PANCN873	3.43 ± 0.19	GN773	6.67 ± 0.14
PANCN1073	3.86 ± 0.14	GN873	7.78 ± 0.14
PANC	4.59 ± 0.06	GN1073	9.33 ± 0.15
PAN−Na	9.67 ± 0.09	G209	10.11 ± 0.16
		G210	9.46 ± 0.11
		G212	10.66 ± 0.19

adsorbed corresponding to the isotherm plateaus $H_2(n_m)$. The data for the maximum amounts of hydrogen adsorbed at 77 K, $H_2(n_m)$, for the carbons used in this study are given in Table 3. $H_2(n_m)$ for the PAN carbon series covered the range 2.89−9.67 mmol g^{-1} (0.58−1.95 wt%), while the range for the G carbon series was 5.85−10.66 mmol g^{-1}(1.18−2.15 wt%). Both the G and PAN series of carbons have very similar micropore and total volumes within each series but widely varying oxygen contents. The amounts of hydrogen adsorbed by the PAN series are ~50% of those of the corresponding G series carbons with the same heat treatment temperature, and this is related to differences in the porous structure characteristics. $H_2(n_m)$ for GN is 63% of GN1073, while the porous structure characteristics are very similar. Similarly, $H_2(n_m)$ for PANCN is 75% of

TABLE 4: Virial Parameters for Hydrogen Adsorption on the Carbons at 77 K A_0 and A_1

A_0			
PAN series carbons	A_0, ln (mol g^{-1} Pa^{-1})	G series carbons	A_0, ln (mol g^{-1} Pa^{-1})
PANCN	−13.113 ± 0.015	GN	−13.606 ± 0.025
PANCN573	−13.228 ± 0.014	GN573	−13.596 ± 0.028
PANCN673	−13.135 ± 0.018	GN673	−13.625 ± 0.052
PANCN873	−13.159 ± 0.018	GN773	−13.461 ± 0.035
PANCN1073	−13.380 ± 0.012	GN873	−13.194 ± 0.028
PANC	−12.934 ± 0.043	GN1073	−12.996 ± 0.032
PAN−Na	−13.271 ± 0.027	G209	−12.670 ± 0.011
		G210	−12.975 ± 0.023
		G212	−13.303 ± 0.014

A_1			
PAN series carbons	A_1, g mol^{-1}	G series carbons	A_1, g mol^{-1}
PANCN	−1616.7 ± 7.6	GN	−588.3 ± 7.0
PANCN573	−1559.9 ± 7.1	GN573	−587.9 ± 7.3
PANCN673	−1508.6 ± 8.9	GN673	−554.5 ± 13.1
PANCN873	−1324.2 ± 8.0	GN773	−558.9 ± 8.4
PANCN1073	−1094.1 ± 4.5	GN873	−492.1 ± 5.7
PANC	−960.0 ± 12.7	GN1073	−413.6 ± 5.4
PAN−Na	−377.0 ± 4.2	G209	−391.2 ± 1.8
		G212	−315.9 ± 2.0
		G210	−409.3 ± 3.8

PANCN1073. However, PANCN1073 has a relatively high total functional group content (∼14 wt% daf) compared with GN1073. $H_2(n_m)$ for PANCN is 63% of PANC with both adsorbents having similar pore structure characteristics. PANC has lower total functional group content (∼10 wt% daf). It is evident that $H_2(n_m)$ increases with increasing heat treatment temperature and decreasing oxygen content, although the porous structure characteristics are very similar within a given series.

3.5. Virial Equation. A saturated vapor pressure is not available under supercritical conditions, and hence, it is more difficult to compare isotherms over a temperature range.

The virial equation[28] can be written in the form

$$\ln(n/p) = A_0 + A_1 n + A_2 n^2 + \ldots \quad (4)$$

where n is the amount adsorbed at pressure p and the first virial coefficient A_0 is related to the Henry's law constant, K_H, by the equation $K_H = \exp(A_0)$.[28] K_H is dependent on the interaction between the adsorbent surfaces and the adsorbed gas molecules.[28] In this study, analysis of the data showed that the higher terms (A_2, etc.) in the virial equation can be ignored under conditions of low surface coverage. The values of the first virial coefficient (A_0) reflect adsorbate−adsorbent interactions, whereas the second virial parameter, A_1, is a function of adsorbate−adsorbate interactions. The value for the isosteric heats of adsorption (Qst) at zero surface coverage can be obtained from a graph of A_0 versus $1/T$.

Figure 2a and b shows the virial graphs for hydrogen adsorption on the PAN and G series of carbons at 77 K. The graphs are linear and the values of A_0 and A_1 obtained from these graphs are given in Table 4. The ln(n/p) values at low surface coverage (<∼0.2 wt%) and low pressure (<∼2 kPa) were subject to higher experimental errors and were not included in the virial graphs. The G series of carbons is the simplest to understand, having essentially only oxygen functional groups. A_0 does not change significantly for HTT ≤ 673 K, but is less negative at high HTT (low oxygen content), indicating a higher K_H. The PAN series carbons contain oxygen (2−20 wt% daf)

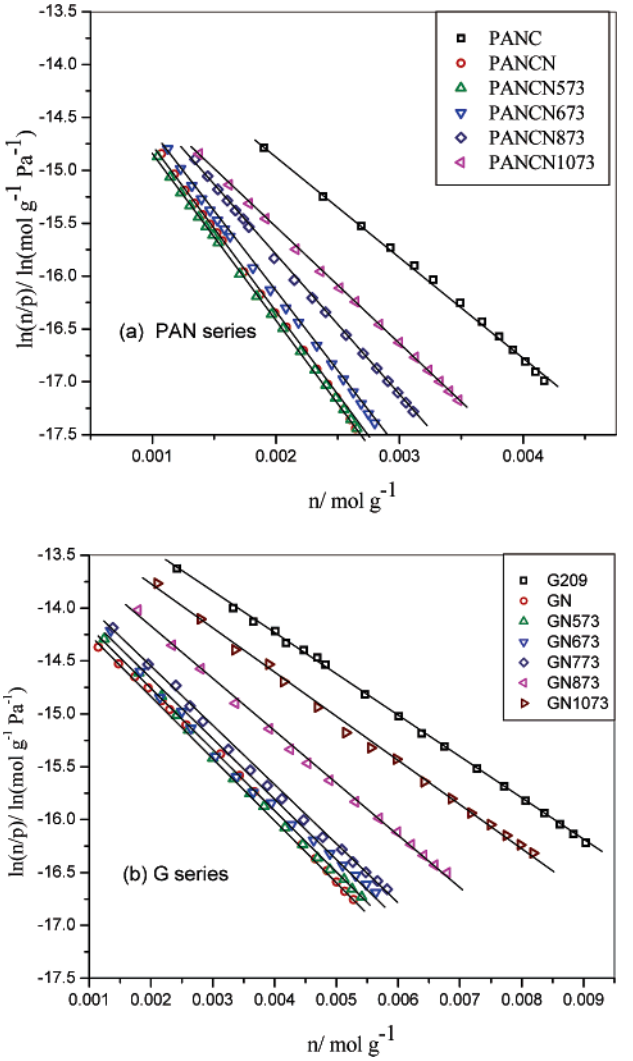

Figure 2. Virial graphs for the adsorption of hydrogen on activated carbons at 77 K (a) PAN series, (b) G series.

and nitrogen, which is constant at ∼8 wt% daf. A_0 does not change significantly for the PAN series up to HTT = 1073 K (PANCN1073), which has a total functional group concentration of ∼14 wt% daf. Carbon PANC, which has an oxygen content of ∼2 wt% daf, has a higher Henry's Law constant similar to the trend in the G series. Therefore, the presence of functional groups decreases the Henry's Law constant in both the G and PAN series, which is related to adsorbate−adsorbent interactions. The second virial parameter, A_1, increases to larger negative values with increasing oxygen content for both series of carbon as shown in Figure 2 and Table 4. Therefore, adsorbate−adsorbate interactions increase with increasing functional group concentrations in both carbon series. Also, it is apparent that the PAN carbon series have more negative values for A_1 than the corresponding G series of carbons. This is related to the higher total functional group concentrations in the PAN carbons due to the nitrogen content. PAN−Na has a mean pore radius intermediate between the G and PAN series of carbons and a much lower nitrogen content (1.76 wt% daf), but has a much lower A_1 value than the other PAN carbons. This also shows that the nitrogen functional groups increase adsorbate−adsorbate interactions. A_0 for PAN−Na is similar to that of the PAN series despite the wider mean pore diameter. It is evident that the virial parameters are strongly dependent on functional group concentrations. Repulsive interactions between functional

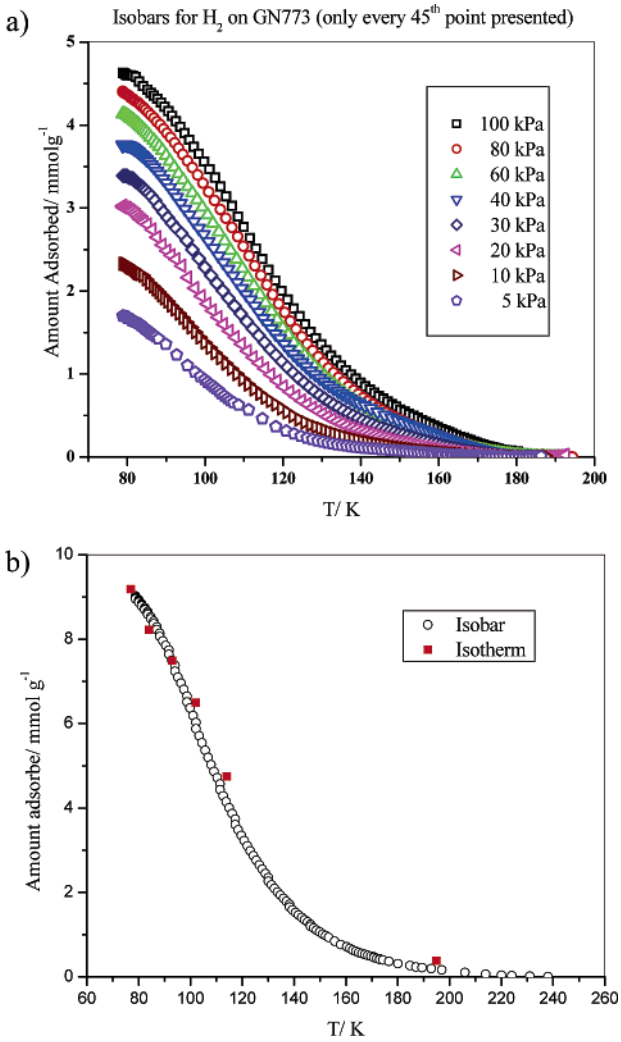

Figure 3. Adsorption isobars for hydrogen desorption (only every 45th point included for clarity) from (a) GN773 at 5−100 kPa and (b) G212 at 100 kPa: heating rate = 0.3 K min^{-1} and (■) 100 kPa data from adsorption isotherms in Figure 1b.

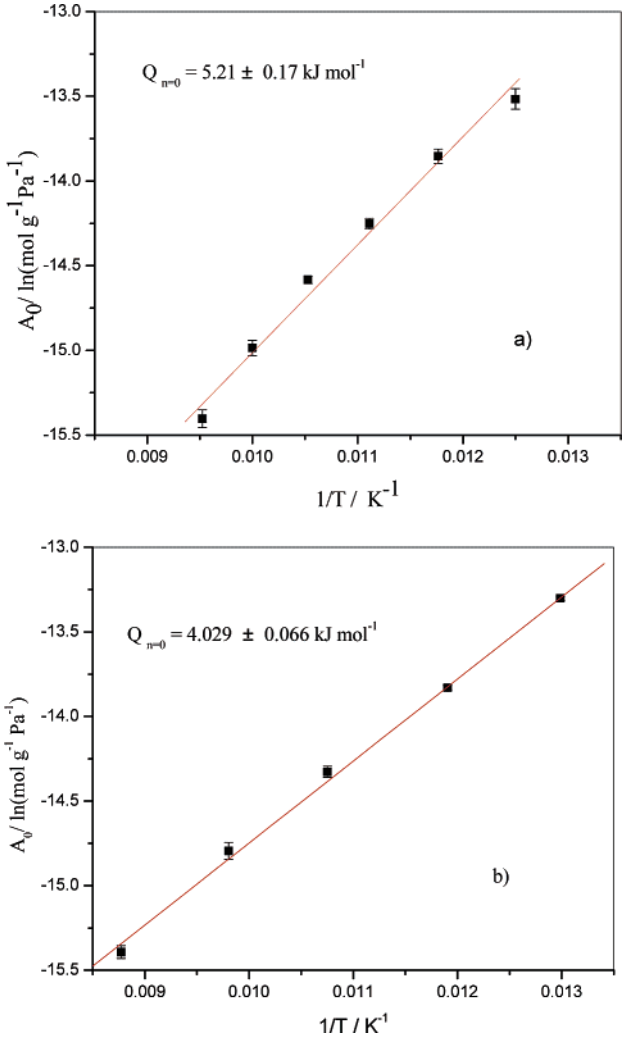

Figure 4. The variation of A_0 with $1/T$ for hydrogen adsorption on (a) GN773 (isobar data) and (b) G212 (isotherm data).

groups and hydrogen molecules lead to increased adsorbate−adsorbate interactions. Electronic effects of functional groups on the graphene layers decrease the adsorbate−adsorbent interactions. The virial parameters (A_1) for hydrogen adsorption at 77 K listed in Table 4 are in the range reported previously for adsorption of argon, oxygen, nitrogen, carbon dioxide, nitrous oxide, carbon monoxide, methane, and ethylene on porous carbons.[28−32]

3.6. Hydrogen Adsorption Isobars. The hydrogen adsorption isotherms are markedly dependent on temperature (see Figure 1b). Therefore, isobars were measured to provide data on the amounts adsorbed as a function of temperature. Initially, the sample adsorption was equilibrated in a predetermined pressure of hydrogen at 77 K. The sample was then allowed to warm naturally by evaporation of the liquid nitrogen. The adsorption kinetics for hydrogen adsorption at 77 K were very fast for all the carbons, and therefore, the samples were in equilibrium at the slow heating rate. Figure 3a shows typical hydrogen adsorption isobars at various pressures for carbon GN773. It is apparent that there is virtually no adsorption of hydrogen above 195 K. Figure 3b compares the hydrogen desorption isobar for G212 at 100 kPa hydrogen pressure with the corresponding isotherm points in Figure 1b. It is evident that there is good agreement, indicating that the desorption method gives a good representation of the isobar for activated carbons. The results indicate that there is little or no adsorption at 195 K.

3.7. Variation of Hydrogen Adsorption as a Function of Temperature. The change in the integral heat of adsorption, Q, with temperature can be described by the following equation:

$$\frac{dQ}{dT} = n_s(Cp_G - Cp_S) \qquad (5)$$

where n_s is the amount adsorbed, Cp_G is the molar heat capacity of the gas phase at constant pressure, Cp_S is the molar heat capacity of the adsorbed phase, and T is the temperature.[33] Therefore, at zero surface coverage, the enthalpy of adsorption is constant and the experimental validation for carbon dioxide adsorption on a carbon molecular sieve (268−580 K) is shown in the Supporting Information. The isosteric enthalpies of adsorption (*Qst*) at zero surface coverage can be obtained from the gradient of the graph of the first virial coefficient (A_0) versus $1/T$.

Graphs of A_0 versus $1/T$ for adsorption of hydrogen on carbons GN773 and G212 are shown in Figure 4. It is apparent that the graphs have a very good linear correlation. The variation of A_1 with temperature for hydrogen adsorption on GN773, G212, and PANCN673 was small over the temperature range studied. The isosteric enthalpies of adsorption at zero surface coverage were obtained from the gradients of the graphs of A_0

versus $1/T$ in Figure 4, and these were 5.21 ± 0.17 and 4.03 ± 0.07 kJ mol^{-1} for GN773 and G212, respectively. The isosteric enthalpy of adsorption at zero surface coverage for PANCN673 obtained from isotherm data was 5.15 ± 0.15 kJ mol^{-1}. It is apparent that the enthalpies of adsorption are similar despite having a wide range of oxygen (1−13 wt%) and nitrogen (0−8 wt%) contents. The isosteric enthalpies of adsorption for hydrogen adsorption obtained from isotherms for G212 in Figure 1b using the van't Hoff isochore were 4.43 ± 0.19, 3.93 ± 0.24, and 3.89 ± 0.31 kJ mol^{-1} at surface coverages of 2, 3, and 4 mmol g^{-1}, respectively. The isosteric enthalpies of adsorption for hydrogen adsorption on PANCN673 obtained using the van't Hoff isochore were 4.76 ± 0.41 and 4.70 ± 0.31 kJ mol^{-1} at surface coverages of 1 and 1.5 mmol g^{-1}, respectively. Also, the isosteric enthalpies of adsorption calculated from the hydrogen isobar data for GN773 in Figure 3a were 4.27 ± 0.28 and 4.12 ± 0.37 at 2 and 3 mmol g^{-1} surface coverage, respectively. It is apparent that there is good agreement between the isosteric enthalpies of adsorption calculated by the various methods and literature values for activated carbons (5−6.5 kJ mol^{-1}),[34,35] thereby confirming the validity of the measurements.

3.8. Hydrogen Adsorption and Porous Structure. The density of adsorbed hydrogen is not known. Comparison of hydrogen adsorption at 20 K and nitrogen at 77 K on single-walled nanohorns (SWNHs) indicated[36] that the average density of adsorbed hydrogen inside SWNHs at 20 K was higher than that of liquid hydrogen in the bulk and nearly approaches the density of solid hydrogen at the triple point.[19] The solid-like behavior of adsorbed hydrogen was attributed to quantum effects.[36] The maximum amounts of hydrogen adsorbed, H_2-(n_m) were converted to a volume of adsorbate using the density of hydrogen at the triple point, 0.077 g cm^{-3} at 13.8 K.[19] The density of the adsorbed phase at 77 K, which is above the critical temperature (33 K), is probably lower than this value. The variation of maximum volume of hydrogen adsorbed with micropore volume determined from extrapolation of the Dubinin−Radushkevich equation for the carbon dioxide adsorption data is shown in Figure 5a. It is evident that there is a linear correlation (intercept −0.022 ± 0.018, gradient 0.847 ± 0.077, $R^2 = 0.896$) which passes through the origin within experimental error. This trend is clearer when only the high-temperature low-oxygen-content carbons are compared, but the correlation parameters are not significantly different. The micropore volume can be converted to a surface area and, therefore, is consistent with the correlation between hydrogen adsorption and surface area.[37] The correlation of $H_2(n_m)$ with total pore volume obtained from nitrogen adsorption at 77 K is less well-defined (intercept 0.003 ± 0.055, gradient 1.66 ± 0.23, $R^2 = 0.79$), as shown in Figure 5b. The results suggest that only the micropore volume is filled with hydrogen at 77 K.

3.9. Hydrogen Adsorption and Functional Groups. The GN−GN1073 series of carbons have an average micropore volume of 0.246 ± 0.016 cm^{3}g^{-1}, while PANCN−PANCN1073 and PANC have an average of 0.134 ± 0.016 cm^{3}g^{-1}. The O/C ratios vary in the range 0.02−0.22 in these samples. This allows the variation of hydrogen adsorption with oxygen functional group content to be studied without the influence of differences in porous structure. The variation of the maximum hydrogen adsorbed, $H_2(n_m)$, determined from the Langmuir isotherm, with O/C ratio for both series is shown Figure 6. It is evident that $H_2(n_m)$ decreases with increasing O/C ratio, and this trend is also observed when $H_2(n_m)$ is considered on a carbon-only basis. CO_2 is the main thermal decomposition of GN and PANCN

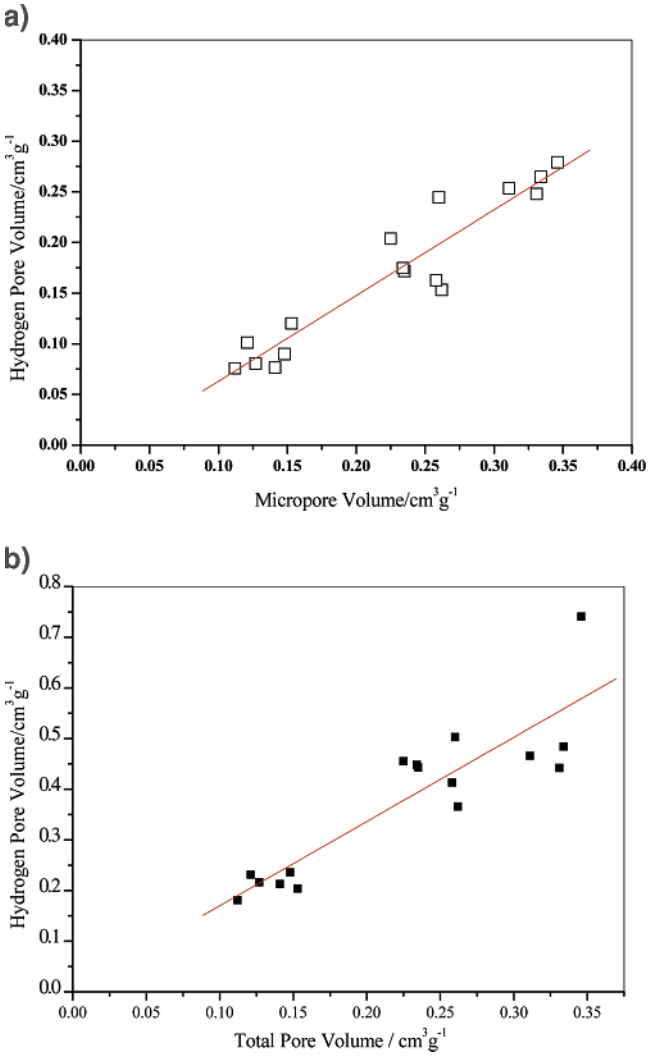

Figure 5. (a) The variation of hydrogen pore volume obtained from hydrogen adsorption at 77 K versus micropore volume obtained from carbon dioxide adsorption at 273 K. (b) The variation of hydrogen pore volume obtained from hydrogen adsorption at 77 K versus total pore volume obtained from nitrogen adsorption at 77 K.

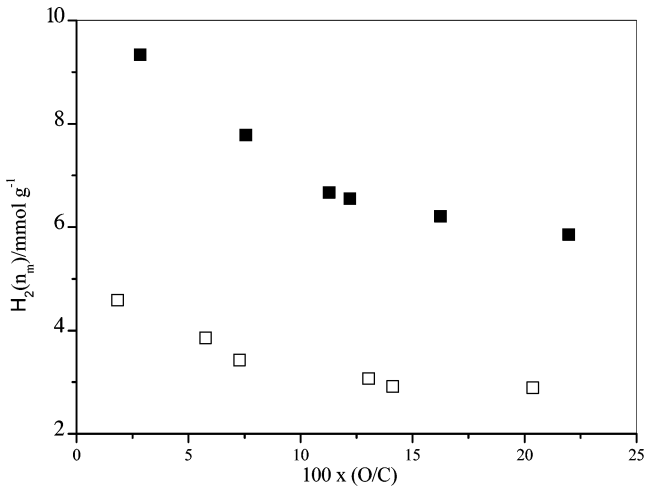

Figure 6. The variation of maximum amount of hydrogen adsorbed (n_m) versus O/C ratio: □, G series; ■, PAN series.

below 673 K, and this is derived from the decomposition of carboxylic groups.[20,21] $H_2(n_m)$ for carbons heat-treated up to this temperature increases to a small extent, and this is consistent with calculations of the interaction energies of H_2 with

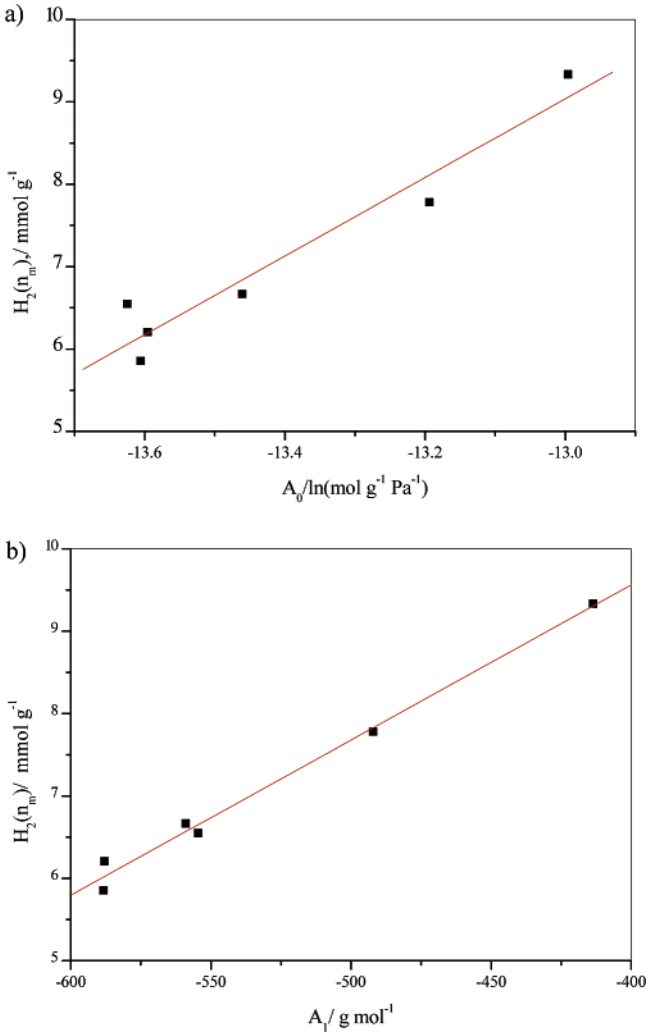

Figure 7. The variation of $H_2(n_m)$ with virial parameters for hydrogen adsorption on GN-GN1073 at 77 K, (a) A_0 and (b) A_1.

substituted aromatic systems.[38] $H_2(n_m)$ has a linear correlation with the virial parameter A_0 with regression coefficient $R^2 = 0.934$. This shows that the maximum amount of hydrogen adsorbed on the isotherm plateau correlates with the Henry's Law constant for the initial uptake region of the isotherm for G series of carbons (see Figure 7a). The A_1 virial parameters for the G series are relatively small, in the range -400 to -600 g mol^{-1} and also have a linear correlation with A_0. Therefore, $H_2(n_m)$ has a linear correlation with the virial parameter A_1 (see Figure 7b) and the regression coefficient $R^2 = 0.990$, which is better than the correlation between $H_2(n_m)$ and A_0. This illustrates the importance of adsorbate−adsorbate repulsive interactions at high oxygen content.

The PAN series of carbons contain both basic nitrogen and acidic oxygen functional groups, which give amphoteric surface properties. A_0 does not change significantly for hydrogen adsorption on PANCN−PACN1073, and this is probably a result of the higher total functional group concentration compared with the corresponding carbons in the G series and the amphoteric surface characteristics. The Henry's Law constant, K_H, for PANC is higher, and this is probably due to the lower oxygen concentration compared with PANCN−PACN1073. The corresponding A_1 virial parameters for the PAN series are larger than the G series in the range -1000 to -1600 gmol^{-1}. In the PAN series, $H_2(n_m)$ has a linear correlation with the second virial parameter (A_1) with $R^2 = 0.956$, as shown in Figure 8. A_1 also increases with increasing oxygen content for the PAN series.

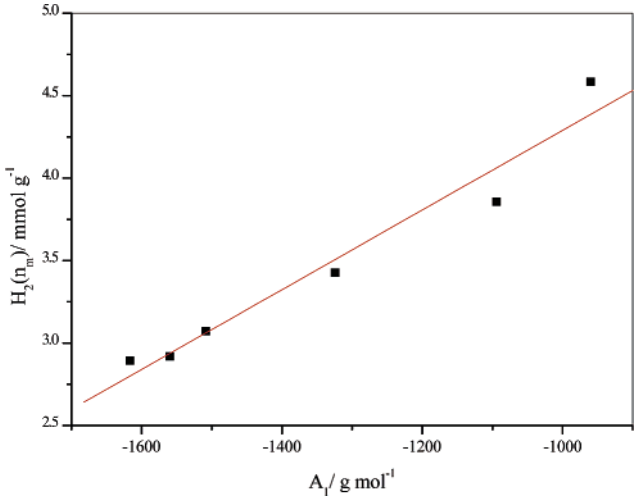

Figure 8. The variation of $H_2(n_m)$ with virial parameter A_1 for hydrogen adsorption on PANCN−PANCN1073 and PANC at 77 K.

Hence, hydrogen adsorption is dominated by the larger adsorbate−adsorbate interactions in the PAN series of carbons. It is apparent that increasing functional group content in carbons decreases adsorbate−adsorbent and increases adsorbate−adsorbate interactions. Hence, functional groups have a negative effect on hydrogen adsorption on activated carbons.

4. Conclusions

This study has shown hydrogen adsorption/desorption on microporous carbons under supercritical conditions at low temperature is reversible with little or no hysteresis. The observation of a constant isosteric enthalpy for hydrogen adsorption at zero surface coverage on porous carbons, derived from a virial equation analysis, is consistent with thermodynamic considerations and also from calculations based on the van't Hoff isochore. The sensitivity of hydrogen adsorption on activated carbon to temperature is very marked, and the amount adsorbed is minimal at 195 K and 100 kPa. This is entirely consistent with the thermodynamic parameters. The maximum amount of hydrogen adsorbed at 77 K correlates with the micropore volume of the carbon. The presence of functional groups has a detrimental effect on the maximum amount of hydrogen adsorption. This is attributed to the decrease in the adsorbate−adsorbent and increase in adsorbate−adsorbate interactions with increasing functional group concentrations. The former is due to electronic effects and the latter to repulsive interactions between hydrogen molecules and functional groups.

Acknowledgment. This paper was prepared by the authors with support from the Carbon Trust. The publication of this paper should not be taken as implying endorsement by the Carbon Trust of any views expressed in the paper or of the services or of the service providers referred to in the paper. The Carbon Trust accepts no liability for the accuracy or completeness of, or omissions from, the contents of the paper or for any loss arising from reliance on it. The authors would like to thank John Holden of Hilltech Developments Ltd for discussions and interest in the research.

Supporting Information Available: Adsorption isotherms. This material is available free of charge via the Internet at http://pubs.acs.org.

References and Notes

(1) *Grand challenge for basic and applied research on hydrogen storage: statement of objectives*; www.eere.energy.gov/hydrogenandfuelcells/docs/gc_h2_storage.doc.

(2) Dillon, A. C., Jones, K. M., Bekkedahl, T. A., Kiang, C. H., Bethune, D. S., Heben, M. J. *Nature (London)* **1997**, *386*, 377.
(3) Chambers, A.; Park, C.; Baker, R. T. K.; Rodriguez, N. M. *J. Phys. Chem. B* **1998**, *102*, 4253.
(4) Park, C.; Anderson, P. E.; Chambers, A.; Tan, C. D.; Hidalgo, R.; Rodriguez, N. M. *J. Phys. Chem. B* **1999**, *103*, 10572.
(5) Chen, P.; Wu, X.; Lin, J.; Tan, K. L. *Science* **1991**, *285*, 91.
(6) Ye, Y.; Ahn, C. C.; Ratnakumar, B. V.;, Witham, C., Jr.; Bowman, R. C.; Fultz, B. *Appl. Phys. Lett.* **1998**, *73*, 3378.
(7) Pinkerton, F. E.; Wicke, B. G.; Olk, C. H.; Tibbets, G. G.; Meisner, G. P.; Meyer, M. S.; Herbst, J. F. *J. Phys. Chem. B* **2000**, *104*, 9460.
(8) Schimmel, H. G.; Kearly, G. J.; Nijkamp, M. G.; Visser, C. T.; de Jong, K. P.; Mulder, F. M. *Chem. Eur. J.* **2003**, *9*, 4764.
(9) Gundiah, G.; Govindaraj, A.; Rajalakshmi, N.; Dhathathreyan, K. S.; Rao, C. N. R. *J Mater. Sci.* **2003**, *85*, 209.
(10) Nijkamp, M. G.; Raaymakers, J. E. M.; van Dillen, A. J.; de Jong, K. P. *Appl. Phys. A* **2001**, *72*, 619.
(11) Becher, M.; Haluska, M.; Hirsher, M.; Quintel, A.; Skakalova, V.; Dettlaff-Weglikovska, U.; Chen, X.; Hulman, M.; Choi, Y.; Roth, S.; Meregalli, V.; Parrinello, M.; Strobel, R.; Jorissen, L.; Kappes, M. M.; Fink, J.; Zuttel, A.; Stepanek, I.; Bernier, P. R. C. *C. R. Phys.* **2003**, *4*, 1055
(12) Rowsell, J. L. C.; Millward, A. R.; Park, K. S.; Yaghi, O. M. *J. Am. Chem. Soc.* **2004**, *126*, 5666.
(13) Ferey, G.; Latroche, M.; Serre, C.; Millange, F.; Loiseau, T.; Percheron-Guegan, A. *Chem. Commun.* **2003**, 2976.
(14) Dybtsev, D. N.; Chun, H.,; Yoon, S.-H.; Kim, D.; Kim, K. *J. Am. Chem. Soc.* **2004**, *126*, 32.
(15) Pan, L.; Sander, M. B.; Huang, X.; Li, J.; Smith, M.; Bittner, E.; Bockrath, B.; Johnson, J. K. *J. Am. Chem. Soc.* **2004**, *126*, 1308.
(16) Zhao, X; Xiao, B.; Fletcher, A. J.; Thomas, K. M.; Bradshaw, D.; Rosseinsky, M. J. *Science* **2004**, *306*, 1012.
(17) Benham, M. J.; Ross, D. K. *Z. Phys. Chem.* **1989**, *163*, 25.
(18) Fletcher, A. J.; Thomas, K. M. *Langmuir* **2000**, *16*, 6253.
(19) CRC *Handbook of Chemistry and Physics*, 74th ed.; CRC Press: Boca Raton, FL, 1993.
(20) Jia, Y. F.; Xiao, B.; Thomas, K. M. *Langmuir* **2002**, *18*, 470.
(21) Xiao, B.; Boudou, J. P.; Thomas, K. M. *Langmuir* **2005**, *21*, 3400−3409.
(22) Boehm, H. P. Carbon **1994**, *32*, 759.
(23) Sing, K. S. W.; Everett, D. H.; Haul, R. A. W.; Moscou, L.; Pierotti, R. A.; Rouquerol, J.; Siemieniewska, T. *Pure Appl. Chem.* **1985**, *57*, 603.
(24) Dubinin, M. M. In *Characterisation of Porous Solids*; Sing, K. S. W., Ed; Society of Chemical Industry: London, 1979; Vol. 1, pp 1−11.
(25) Dubinin, M. M.; Stoeckli, H. F. *J. Colloid Interface Sci.* **1980**, *75*, 34.
(26) Yaris, R.; Sams, J. R., Jr. *J. Chem. Phys* **1962**, *37*, 571.
(27) Langmuir, I. *J. Am. Chem. Soc.* **1918**, *40*, 1361.
(28) Cole, J. H.; Everett, D. H.; Marshall, C. T.; Paniego, A. R.; Powl, J. C.; Rodriguez-Reinoso, F. *J. Chem. Soc., Faraday Trans. 1* **1974**, *70*, 2154.
(29) Reid, C. R.; O'Koye, I. P.; Thomas, K. M. *Langmuir* **1998**, *14*, 2415.
(30) O'koye, I. P.; Benham, M.; Thomas, K. M. *Langmuir* **1997**, *13*, 4054.
(31) Reid, C. R.; Thomas, K. M. *Langmuir* **1999**, *15*, 3206.
(32) Reid, C. R.; Thomas, K. M. *J. Phys. Chem. B* **2001**, *105*, 10619.
(33) Cerny, G. *Chem. Phys. Solid Surf. Heterog. Catal.* **1983**, *2*, 1.
(34) P. Bernard, P.; Chahine, R. *Langmuir* **2001**, *17*, 1950.
(35) Zhou, L.; Zhou, Y.; Sun, Y. *Int. J. Hydrogen Energy* **2004**, *29*, 475.
(36) Tanaka, H.; Kanoh, H.; El-Merraoui, M.; Steele, W. A.; Yudasaka, M.; Iijima, S.; Kaneko, K. *J. Phys. Chem. B* **2004**, *105*, 10619.
(37) Pang, J.; Hampsey, J. E.; Wu, Z.; Hu, Q.; Lu, Y. *Appl. Phys. Lett.* **2004**, *85*, 4887.
(38) Hubner, O.; Gloss, A.; Fitchner, M.; Klopper, W. *J. Phys. Chem. B* **2004**, *108*, 3019.